Spin-Polarization transition in the two dimensional electron gas

D. Varsano[1], S. Moroni[1] and G. Senatore[2]

[1] *INFM, Università di Roma "La Sapienza" - P.le Aldo Moro 2, 00185, Roma, Italy*
[2] *INFM, Dipartimento di Fisica Teorica, Università di Trieste - Strada Costiera 11, 34014, Trieste, Italy*

PACS. 71.10.Ca – .
PACS. 05.30.Fk – .
PACS. 75.30.Kz – .

Abstract. – We present a numerical study of magnetic phases of the 2D electron gas near freezing. The calculations are performed by diffusion Monte Carlo in the fixed node approximation. At variance with the 3D case we find no evidence for the stability of a partially polarized phase. With plane wave nodes in the trial function, the polarization transition takes place at $r_s = 20$, whereas the best available estimates locate Wigner crystallization around $r_s = 35$. Using an improved nodal structure, featuring optimized backflow correlations, we confirm the existence of a stability range for the polarized phase, although somewhat shrunk, at densities achievable nowadays in 2 dimensional hole gases in semiconductor heterostructures . The spin susceptibility of the unpolarized phase at the magnetic transition is approximately 30 times the Pauli susceptibility.

Quantum simulations show that the three–dimensional electron gas undergoes a continuous spin-polarization transition, upon decreasing the density into the strongly correlated regime, before forming a Wigner crystal [1, 2]. Despite the theoretical interest of a simple model exhibiting quantum phase transitions [3], the difficulty of realizing a low density electron gas in real materials makes the contact with experiment a rather indirect one [4]. However, electrons can be confined into effectively two–dimensional systems, for instance in Si MOSFET's and III-V semiconductor heterostructures [5], over a density range extending down to the freezing transition [6].

Far from being a mere playground for testing many–body theories and numerical simulations, strongly correlated two–dimensional electronic systems offer an extremely rich and interesting phenomenology, such as the fractional quantum Hall effect [7] and a previously unexpected metal–insulator transition [8], not to mention their relevance to superconductor cuprates [9]. Therefore, we think that it is useful to extend the work of ref. [2] and study the polarization transition of the two–dimensional electron gas (2DEG). In fact, spin fluctuations appears to play an important role in the 2DEG at the metal–insulator transition in presence of disorder [10]).

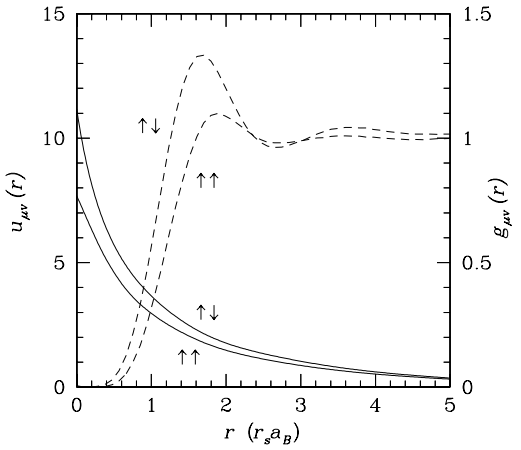

Fig. 1 – Optimized pseudopotentials $u_{\mu\nu}(r)$ (solid lines,left scale) and VMC pair distribution functions $g_{\mu\nu}(r)$ (dashed line, right scale) for the unpolarized 2DEG at $r_s = 20$.

Previous quantum Monte Carlo (QMC) simulations [11–15] of the 2DEG provide little information on the magnetic properties of the system, with only one spin susceptibility calculation [15] at non–zero wave vectors and relatively high densities ($r_s \leq 10$, where $r_s a_B = 1/\sqrt{\pi\rho}$ with a_B the Bohr radius and ρ the density), and one attempt at exploring the partially polarized case [11] near freezing. We emphasize that we have only mentioned, here, results obtained from QMC, a computationally demanding numerical method which projects the ground state from a trial function Ψ_T by a stochastic technique [16]. Both in this work and in refs. [2,11–15] the method is implemented in the fixed–node (FN) approximation [17], giving the lowest upper bound to the ground state energy consistent with the *nodal structure* of Ψ_T. Though not exact unless Ψ_T has the same nodes as the unknown ground state, a condition not generally met, FN–QMC provides fairly accurate predictions for ground state properties of interacting fermion systems. Other approximate theories may fulfill such an accuracy requirement at weak coupling [19], but are not amenable to systematic improvement in the strongly correlated regime. When applied beyond their range of validity, they predict a variety of magnetic instabilities at unrealistically high densities [20].

We simulate 2D systems of $N = N_\uparrow + N_\downarrow$ electrons, interacting with a pair potential $v(r) = 2/(r_s r)$, in a square box of side $L = \sqrt{N\pi}$ with periodic boundary conditions (energies are in Ry and distances in $r_s a_B$ units). A rigid uniform background of positive charge ensures neutrality. The polarization is $\zeta = (N_\uparrow - N_\downarrow)/N$. Following ref. [2], we use a Jastrow–Slater form for the trial function, $\Psi_T = \exp[-\sum_{i<j} u_{\mu\nu}(r_{ij})] D_\uparrow D_\downarrow$. Here the indices i, j label electrons, μ and ν label the spin of particles i and j; $u(r)_{\mu\nu}$ are pair pseudopotentials for like ($\mu = \nu$) or unlike–spin ($\mu \neq \nu$) particles, optimized for each system considered, and $D_{\uparrow(\downarrow)}$ is a Slater determinant of plane waves for up(down)–spin electrons. As it has been previously done in three dimension [1, 2], we are only considering homogeneous phases [18].

Figure 1 shows the optimized pseudopotentials for an unpolarized system with $N = 114$ at $r_s = 20$. In the same figure, the spin–resolved pair distribution functions $g_{\uparrow\uparrow}(r)$ and $g_{\uparrow\downarrow}(r)$, computed with variational Monte Carlo (i.e. by taking the expectation value over $|\Psi_T\rangle$) is shown by the dashed lines. Despite the fact that the like–spin pseudopotential is less repulsive,

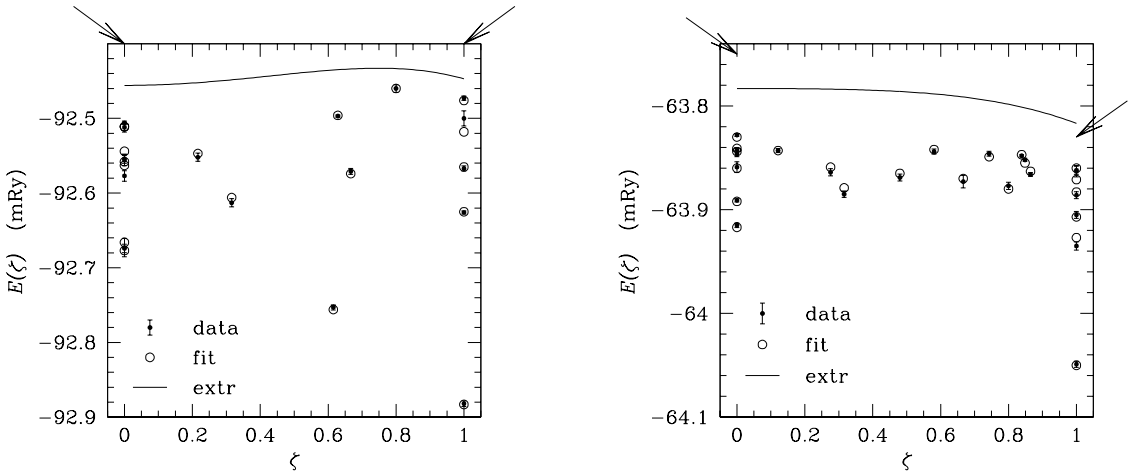

Fig. 2 – Plane wave fixed node energy versus polarization at $r_s = 20$ (left panel) and at $r_s = 30$ (right panel).

the pair distribution functions do not show the local ferromagnetic order predicted [2] in 3D across the magnetic transition. Note that in 2D, at the accuracy level of FN–QMC with plane wave determinants, the energies of the unpolarized and the fully polarized phases cross precisely at $r_s = 20$, according to both ref. [14] and the present work (see below).

Our estimate of energy vs. polarization in the thermodynamic limit, parametrized in the form $E(\zeta) = E(\zeta = 0) + \beta\zeta^2 + \gamma\zeta^4$, is shown by the solid line for $r_s = 20, 30$, in fig. 2. The statistical uncertainty is less than 10^{-5}. The points with errorbars are FN–QMC results with plane waves, and the open circles are the result of the fit for the number extrapolation (see below). The arrows indicate the results of ref. [14] at $\zeta = 0$ and $\zeta = 1$.

The polarized and unpolarized phases have nearly the same energy at $r_s = 20$, whereas at $r_s = 30$ the polarized fluid is stable. We find no evidence for the stability of a partially polarized phase at these densities, and we believe that this is the case for other densities as well (a reentrant partially polarized phase could form for $r_s < 20$; alternatively, γ should change sign twice [21] between $r_s = 20$ and $r_s = 30$: both cases seem unlikely). This conclusion agrees with a conjecture of ref. [11], based on the simulation of a single partially polarized system at $r_s = 40$; however, the more systematic analysis presented here seems worth the effort, also in view of some discrepancies existing between the results of ref. [11] and later simulations [13, 14].

The dispersion of the FN $E(\zeta)$ is very weak, which reflects in a large spin susceptibility χ_s of the unpolarized 2DEG at $r_s = 20$, where the first–order polarization transition takes place. The best–fit value of β is $8.2 \pm 1.2 \times 10^{-5}$, corresponding to $\chi_s/\chi_P \simeq 30$, where χ_P is the Pauli susceptibility. This is an extremely large value of χ_s. We note that a phenomenological model for χ_s [22], based on including known sum rules and fitting QMC data from ref. [11], gives $\chi_s/\chi_P = 1.6$ at $r_s = 20$.

We now discuss the differences between our results and the ones of refs. [13, 14] (all three calculations are nominally equivalent). We perform QMC simulations in the Diffusion Monte Carlo (DMC) version [23]. A population of N_W walkers (copies of the system) perform a random walk in configuration space. The time steps of the random walk stochastically follow

TABLE I – *Energy–fitting parameters from DMC. See text for the meaning of symbols*

	$E(\zeta=0)$	$\beta\times10^5$	$\gamma\times10^5$	Δ	ϵ	b	α	χ^2
$r_s=20$	-0.092456	8.22	-7.34	0.00129	2.0	0.00712	-0.0030	1.7
$r_s=30$	-0.063783	-0.64	-2.72	0.00045	1.8	0.00397	-0.0007	1.9

a short time approximation to the imaginary time evolution of the quantum system. The results need to be extrapolated to zero time step τ and, in the implementation used, to infinite N_W, as well as to the standard thermodynamic limit $N\to\infty$. In brief, (i) we perform the number extrapolation directly on several DMC energies instead of sticking the VMC size corrections on the DMC energy computed for a single system size [13,14], and (ii) we believe that we better control the finite τ and finite N_W biases.

We fit the energies computed at various polarizations ζ and particle numbers N using

$$E_N(\zeta)=E(\zeta=0)+\beta\zeta^2+\gamma\zeta^4+\Delta(1+\epsilon\zeta^2)(T_N^{(0)}(\zeta)-T^{(0)}(\zeta))-(b+\alpha\zeta^2)/N, \qquad (1)$$

where $T_N^{(0)}$ and $T^{(0)}$ are the kinetic energies of a non–interacting 2DEG at $r_s=1$ for N particles and in the thermodynamic limit, respectively. The fitting parameters from FN energies with plane wave nodes are listed in table I. Obviously, the fit to the VMC energies yields different values for $E(\zeta=0)$, β and γ. Less obvious is the difference of the other fitting parameters (i.e. is the number extrapolation the same for DMC as for VMC?). In table II we list the fitting parameters obtained from VMC (103 systems at each density using parameter-free RPA pseudopotentials [24] to avoid spurious effects from different levels of optimization at different particle numbers). This VMC–DMC comparison may be in part biased by the fact that we used Ewald sums [25] for the Coulomb potential in VMC, and a truncated potential [26] in DMC. However we note that b, the fitting parameter directly related to the potential energy, is nearly the same in VMC and DMC, a significant difference being instead present in the kinetic energy terms.

We turn now to the time step error and the population control bias. The results for $r_s=20$ shown in fig. 2 are all extrapolated at infinite number of walkers and zero time step. For $r_s=30$ the extrapolation has been done in 10 cases; then a time step $\tilde\tau$ and a number of walkers $\tilde N_W$ have been chosen such that the residual bias is less than 5×10^{-6} in the selected cases. Some of the results shown in fig. 2 for $r_s=30$ are obtained using $\tilde\tau$ and $\tilde N_W$.

For 58 particles at $r_s=20$, both ref. [14] and [13] report $E=-0.09248(1)$. However we find that the extrapolation at zero time step and infinite number of walkers is $-0.092557(76)$. In fig. 3 the results for various numbers of walkers and time steps are shown by star symbols. For each τ the extrapolation (linear in $1/N_W$) to infinite number of walkers is shown by the diamond. The extrapolation (linear in τ) of the diamonds to zero time step is shown by the open circle. The shaded region encloses the energy values between -0.09248 ± 1, i.e. it represents the result of refs. [13,14].

The filled circle indicates a result, extrapolated to $\tau=0$ and $N_W=\infty$, obtained with a

TABLE II – *Energy–fitting parameters from VMC. See text for the meaning of symbols*

	$E(\zeta=0)$	$\beta\times10^5$	$\gamma\times10^5$	Δ	ϵ	b	α	χ^2
$r_s=20$	-0.091553	-30.2	-60.7	0.00258	1.0	0.00687	0.0026	2.3
$r_s=30$	-0.063237	-52.3	-43.0	0.00090	2.1	0.00355	0.0009	2.8

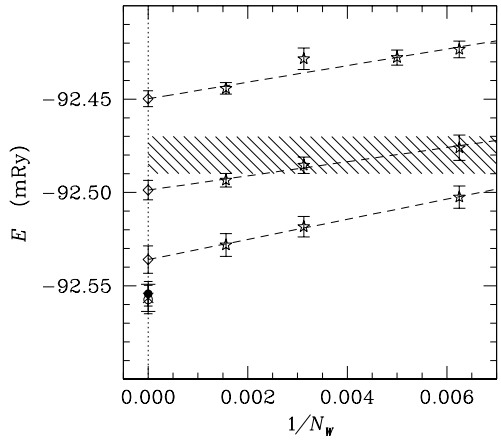

Fig. 3 – Effects of finite time step and number of walkers on the fixed node energy for 58 particles at $r_s = 20$, in the normal fluid. See text for the meaning of symbols

different DMC code, in which walkers carry a weight for a while and branch every so often [27] instead of branching at each time step. The cross is the result, extrapolated to $\tau = 0$, of yet another calculation with reptation QMC [28], a single–thread algorithm (hence, one having no population control bias). The finite–τ and finite–N_W biases are all different in these calculations, but the extrapolated result is the same. This cross–check performed using three different algorithms gives us confidence on our extrapolated results.

The above analysis demonstrates the importance of an extremely accurate control of the convergence parameters of the numerical calculations, due to the relevance of small energy differences on physical properties related to spin polarization in this strongly coupled system.

We finally consider the FN approximation. In 3D, the error of the FN energies with plane wave nodes is presumably negligible [2] in characterizing the continuous polarization transition. On the energy scale of the weak dependence of E on ζ shown in figs. 2, however, the FN bias might be relevant. We have computed FN energies with better nodes provided by optimized backflow correlations [29], at $r_s = 20$ and 30 for zero and full polarization. Where available, comparison between the FN energy with backflow nodes and the exact result [30] supports the accuracy of the former for the 2DEG. Including backflow correlations, the FN energy decreases more for $\zeta = 0$ than for $\zeta = 1$: the relative gain of the unpolarized phase is found to be $7.2(7) \times 10^{-5}$ at $r_s = 20$ and $2.0(9) \times 10^{-5}$ at $r_s = 30$. This makes the unpolarized phase stable at $r_s = 20$, but at $r_s = 30$ the energy of the polarized fluid remains lower (compare with fig. 2 and table I), even though by an amount close to the statistical uncertainty [31].

At $r_s = 30$ the system is still fluid. Based on plane wave FN energies, crystallization occurs at a lower density, $r_s = 37 \pm 5$ and 34 ± 4 according to refs. [11] and [14], respectively. In fact, backflow correlations will further stabilize the fluid phases, likely yielding a slightly lower crystallization density (for the polarized liquid at $r_s = 30$ we find a tiny difference of $1.6(4) \times 10^{-5}$ between the plane wave and the backflow FN energy).

Summarizing, we have studied the polarization transition in the 2DEG using the FN–DMC method. With plane wave nodes, the transition is first order and takes place at $r_s = 20$, where

the spin susceptibility reaches $30\chi_P$. Upon improvement of the nodal structure, obtained including backflow correlations, the transition density approaches $r_s = 30$, still leaving a stability window for the fully polarized phase between the paramagnetic fluid and the Wigner crystal.

* * *

We acknowledge support from INFM under the Parallel Computing Initiative and from MURST under the PRIN 1999 Initiative.

REFERENCES

[1] Alder B.J., Ceperley D.M. and Pollock E.L., *Int. J. Quantum Chem.*, **16** (1982) 49.
[2] Ortiz G., Harris M. and Ballone P., *Phys. Rev. Lett.*, **82** (1999) 5317.
[3] Sondhi S.L., Girvin S.M., Carin J.P. and Shahar D., *Rev. Mod. Phys.*, **69** (1997) 315.
[4] Young D.P. *et al.*, *Nature*, **397** (1999) 412; Ceperley D.M., *ibid.,* 386.
[5] Ando T., Fowler A.B. and Stern F., *Rev. Mod. Phys.*, **54** (1982) 437.
[6] Yoon J *et al.*, *Phys. Rev. Lett.*, **82** (1999) 1744.
[7] Tsui D.C., Störmer H.L. and Gossard A.C, *Phys. Rev. Lett.*, **48** (1982) 1559.
[8] Kravchenko S.V. *et al.*, *Phys. Rev. B*, **51** (1995) 7038.
[9] Bednorz J.R. and Müller K.A., *Z. Phys. B*, **64** (1986) 189.
[10] Belitz D. and Kirkpatrick T.R., *Rev. Mod. Phys.*, **66** (1994) 261; Castellani C., Di Castro C. and Lee P.A., *Phys. Rev. B*, **57** (1998) R9381; see, also, Castellani C., Di Castro C, Lee P.A., Ma M., Sorella S and Tabet E., *Phys. Rev. B*, **33** (1986) 6169.
[11] Tanatar B. and Ceperley D.M., *Phys. Rev. B*, **39** (1989) 5005.
[12] Moroni S., Ceperley D.M. and Senatore G., *Phys. Rev. Lett.*, **69** (1992) 1837.
[13] Kwon Y., Ceperley D.M. and Martin R.M., *Phys. Rev. B*, **48** (1993) 12037.
[14] Rapisarda F. and Senatore G., *Australian J. Phys.*, **13** (1999) 12.
[15] Senatore G., Moroni S. and Ceperley D.M., *Quantum Monte Carlo Methods in Physics and Chemistry*, edited by M.P. Nightingale and C.J. Umrigar (Kluwer) 1999, p. 183.
[16] Ceperley D.M. and Kalos M.H., in *Monte Carlo Methods in Statistical Physics*, edited by, edited by Binder K. (Springer) 1979; Schmidt K.E. and Kalos M.H., in *Monte Carlo Methods in Statistical Physics II*, edited by, edited by Binder K. (Springer) 1982.
[17] Anderson J.B., *J. Chem. Phys.*, **63** (1975) 1499; *J. Chem. Phys.*, **65** (1976) 4122; Ceperley D.M., in *Recent Progress in Many–Body Theories*, edited by, edited by Zabolitzky J. (Springer) 1981.
[18] We are not considering the possibility of spatial modulations of either charge or spin, i.e., we are disregarding here charge and spin density waves.
[19] Yarlagadda S. and Giuliani G., *Phys. Rev. B*, **40** (1988) 5432.
[20] See e.g. Sato K. and Ichimaru S., *J. Phys. Soc. Japan*, **58** (1989) 787; Mougdil R.K., Ahluwalia P.K. and Pathak K.N., *Phys. Rev. B*, **51** (1995) 1575.
[21] Note that with the chosen form for $E(\zeta)$, an absolute minimum at $0 < \zeta^* < 1$ requires: $\beta < 0$, $\gamma > 0$, and $\gamma > -\beta/2$
[22] Iwamoto N., *Phys. Rev. B*, **43** (1991) 2174.
[23] Reynolds P.J., Ceperley D.M., Alder B.J. and Lester W.A., *J. Chem. Phys.*, **77** (1982) 5593; Umrigar C.J., Nightingale M.P. and Runge K.J., *J. Chem. Phys.*, **99** (1993) 2865.
[24] Ceperley D.M., *Phys. Rev. B*, **18** (1978) 3128.
[25] Natoli V.D. and Ceperley D.M., *J. Comput. Physics*, **117** (1995) 171.
[26] Fraser L.M. *et al.*, *Phys. Rev. B*, **53** (1996) 1814.
[27] See, e.g. Calandra M. and Sorella S., *Phys. Rev. B*, **57** (1998) 11446.
[28] Baroni S. and Moroni S., *Phys. Rev. Lett.*, **82** (1999) 4745.
[29] Schmidt K.E., Lee M.A. and Kalos M.H., *Phys. Rev. Lett.*, **47** (1981) 807.

[30] Kwon Y., Ceperley D.M. and Martin R.M., *Phys. Rev. B*, **53** (1996) 7376.
[31] We should mention that similar conclusions are obtained at $r_s = 30$ by combining the Jastrow–Slater node energies of [14] with unpublished backflow node energies of Kwon [32].
[32] Kwon Y., *unpublished*, (1995) .